



Enhanced activity for gas phase propylene oxide rearrangement to allyl alcohol by Au promotion of Li_3PO_4 catalyst



Xiangshuai Zhu, Dongyu Wang, Zhishan Li, Weihua Ma*

School of Chemical Engineering, Nanjing University of Science and Technology, Nanjing, 210094, PR China

ARTICLE INFO

Keywords:

Nano-gold
Lithium phosphate
pH
Base strength
DFT

ABSTRACT

In present paper, lithium phosphate (Li_3PO_4) promoted by nano-gold (denoted as $\text{Au}/\text{Li}_3\text{PO}_4$) was used in gas phase propylene oxide (PO) rearrangement to produce allyl alcohol (AA). It was found that the support of gold could improve the catalytic activity as compared with pure Li_3PO_4 . $\text{Au}/\text{Li}_3\text{PO}_4$ with gold loading of 0.042 wt% showed higher catalytic performance. The enhancement might come from the increase of the strength and amount of strong basic sites after gold deposition. Results of XPS spectra and density functional theory (DFT) verified that the charge transfer from oxygen species to gold species led to the electron-rich gold species, which acted as stronger base sites.

1. Introduction

The rearrangement of epoxides to carbonyl compounds or allyl alcohols (AA) is a fundamentally important process due to their industrial utility. For instance, the Meinwald rearrangement, which refers to rearrangement of epoxides to carbonyl compounds under acidic conditions, is a fundamentally important transformation [1]. The composition of rearrangement products is determined by the acidic-basic properties of the catalysts [2]. Imanaka et al. have proposed that, in rearrangement of PO, AA is produced by acid-basic bifunctional catalysts, acetone, by basic-site only, and propylaldehyde, by acid-site only [3]. According to previous studies [3–5], we summarized the mechanism of PO conversion pathways for different products in Scheme 1. Therefore, in order to obtain AA, amphoteric oxides including Al_2O_3 , ZrO_2 , TiO_2 [6] or Li_3PO_4 have been used as catalysts for epoxides rearrangement. Li_3PO_4 has been a special catalyst due to high conversion and selectivity for PO rearrangement to AA. There are two processes, i.e., the gas phase and the liquid phase [7]. The gas phase process is much simpler and cleaner than the liquid phase. However, carbon deposition has always been a major problem [8], thus Li_3PO_4 should be further studied and improved.

Gold has been considered as an inert metal and catalytically inactive for a long time [9]. But it was overturned when Haruta and coworkers [10] discovered supported gold catalysts exceedingly active for low-temperature CO oxidation. Since then, much attention has been attracted to gold catalysts. It was likely that a Gold Rush occurred in the field of catalysis [11]. Various applications of gold catalysts have been

discovered to date, such as environmental control, energy processing and chemical synthesis [12,13]. Recently, Raptis et al. [4] found a new application of gold catalyst that Au/TiO_2 could catalyze the rearrangement reaction of epoxides to AA with high yields. But Raptis's work is mainly on the liquid phase process. Our work is on the gas phase process. We supported Au on Li_3PO_4 to catalyze PO and results demonstrated that the support of gold could obviously improve the catalytic activity. From FT-IR, CO_2 -TPD, XPS and DFT, it could be concluded that the enhancement came from the strength and amount of strong basic sites, namely, the electron-rich gold species that charge was transferred from oxygen species.

2. Experimental section

2.1. Preparation of $\text{Au}/\text{Li}_3\text{PO}_4$

A basic Li_3PO_4 was synthesized by 14.5 g lithium hydroxide (LiOH) and 32.8 g sodium phosphate (Na_3PO_4), which were dissolved in deionized water and stirred at 60 °C for 2 h. The resultant was separated by centrifugation and washed several times until the pH decreased to 13, then dried at 100 °C for 5 h and calcined at 320 °C for 6 h with a heating rate of 2 °C min^{-1} . This resulting was denoted as Li_3PO_4 -13. Li_3PO_4 with different pH values, denoted as Li_3PO_4 -x (x = pH), was obtained by adjusting the pH of the slurry of uncalcined Li_3PO_4 aqueous solution to the desired value by 1 M hydrochloric acid (HCl) solution. Gold supported onto Li_3PO_4 -x (denoted as $\text{Au}/\text{Li}_3\text{PO}_4$ -x) was prepared via a

* Corresponding author.

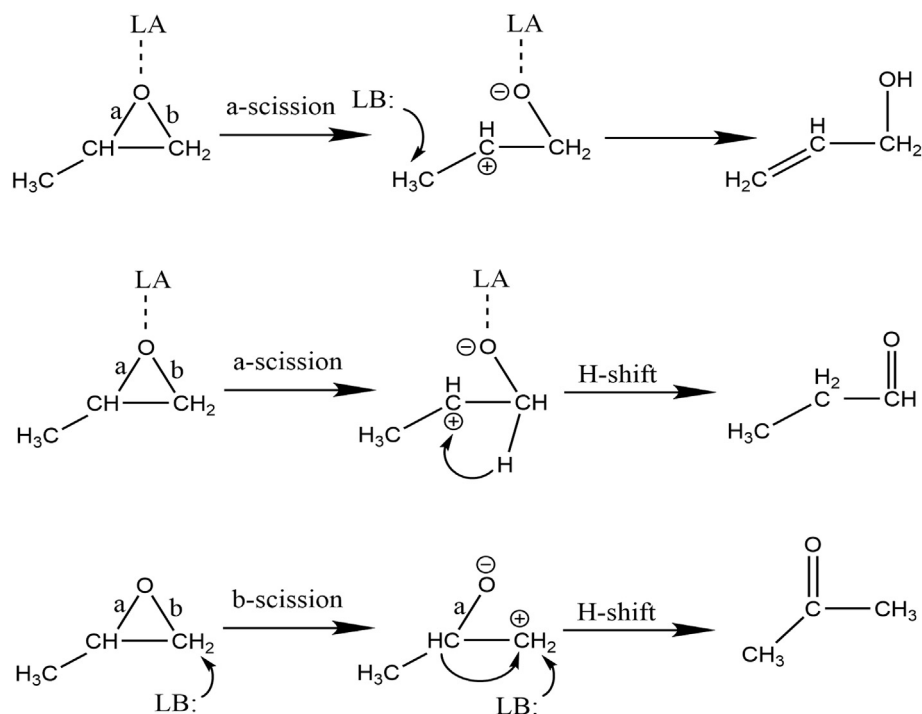
E-mail address: maweihuacn@163.com (W. Ma).

<https://doi.org/10.1016/j.jssc.2019.120922>

Received 20 May 2019; Received in revised form 31 July 2019; Accepted 22 August 2019

Available online 29 August 2019

0022-4596/© 2019 Elsevier Inc. All rights reserved.



Scheme 1. Schematic representation of the different mechanistic pathways for propylene oxide rearrangement. LA = Lewis acid, LB = Lewis base.

deposition precipitation method [14,15]. Approximately 0.1 g $\text{HAuCl}_4 \cdot 4\text{H}_2\text{O}$ was dissolved in 50 mL deionized water and 1.0 g Li_3PO_4 was added with stirring. Afterwards, the pH of the slurry was adjusted to 13 by 1 M sodium hydroxide (NaOH) solution. The suspension was stirred at 80 °C for 2 h and then centrifuged, washed and dried at 100 °C for 5 h. Finally, the product was calcined at 300 °C for 4 h with a heating rate of 2 °C min^{-1} .

2.2. Catalyst characterization

The Brunauer-Emmett-Teller (BET) surface area was determined by N_2 adsorption-desorption measurements at 77 K (Gold App V-sorb 2008). Powder X-ray diffraction (XRD) was carried out with a general X-ray diffraction instrument (Beijing Purkinjie XD-3). TEM experiments were carried out on a Philips Tecnai 12 transmission electron microscope. UV-visible spectra were recorded by a Thermo Scientific Evolution 220 spectrophotometer equipped with an ISA-220 integrating sphere. The gold contents in catalysts were measured by Optima 7300 DV inductively coupled plasma spectrometer (PerkinElmer). FT-IR spectra were recorded by Thermo Scientific Nicolet iS10. X-ray photoelectron spectroscopy (XPS) experiments were carried out on a RBD-upgraded PHI-5000C ESCA system (PerkinElmer) with $\text{Mg K}\alpha$ radiation ($h\nu = 1253.6$ eV), calibrated by the C 1s peak at 284.6 eV. Carbon dioxide temperature-programmed desorption (CO_2 -TPD) experiments were carried out under a flow of He (70 $\text{cm}^3 \text{min}^{-1}$) and the temperature was raised from room temperature to 600 °C at a heating rate of 10 °C min^{-1} . Ammonia gas temperature-programmed desorption (NH_3 -TPD) experiments were carried out under a flow of He (70 $\text{cm}^3 \text{min}^{-1}$) and the temperature was raised from room temperature to 600 °C at a heating rate of 10 °C min^{-1} . The fresh and used catalysts were characterized by thermogravimetric analysis (TG, Mettler-Toledo TGA/SDTA851e) at the rate of 10 °C/min in air (100 ml/min) atmosphere.

2.3. Measurement of catalytic activity

Catalytic performance was determined in a fixed bed reactor under atmospheric pressure. The catalyst (0.3 g, particle diameter of

0.30–0.45 mm) was placed in a fixed-bed reactor with 10 mm in diameter. A mixture of vaporized PO and N_2 (the molar ratio is 0.59) was introduced into the reactor, and the WHSV of propylene oxide was 33.2 h^{-1} . The reaction temperature was controlled at the optimal reaction temperature of 300 °C. The products were condensed using a sample collector settled in ice water bath and analyzed by a SP-1000 Gas Chromatography equipped with PEG-20M capillary column.

3. Results and discussions

3.1. Characterization and catalytic performance of the catalysts

Fig. S1 shows the catalytic performances of $\text{Au}/\text{Li}_3\text{PO}_4$ at different preparation conditions, including gold loading, calcination temperature and pH value of Li_3PO_4 , which are of significance to the catalytic performance of propylene oxide rearrangement to allyl alcohol. As can be seen, $\text{Au}/\text{Li}_3\text{PO}_4$ -13 with gold loading content of 0.042 wt% and calcined at 300 °C, showed the best catalytic performance and was chosen as the catalyst for PO rearrangement reaction. Furthermore, the catalytic performance of $\text{Au}/\text{Li}_3\text{PO}_4$ is sensitive to the pH values. As presented in Table S1, the selectivity to AA has changed greatly at pH = 9, which verified again that higher catalytic activity and selectivity is maintained under strong basic condition.

The physical properties of the $\text{Au}/\text{Li}_3\text{PO}_4$ -13 and Li_3PO_4 -x are listed in Table S2. It can be seen that the surface area of Li_3PO_4 decreases gradually from 26 to 14 $\text{m}^2 \text{g}^{-1}$ as the pH value decreases from 13 to 9. When the gold is deposited on Li_3PO_4 -13, the surface area decreases to 20 $\text{m}^2 \text{g}^{-1}$, which might be due to gold filling in some pores of Li_3PO_4 substrate. When $\text{Au}/\text{Li}_3\text{PO}_4$ -13 was used for 5 h (denoted as $\text{Au}/\text{Li}_3\text{PO}_4$ 5 h), the surface area decreased to 10 $\text{m}^2 \text{g}^{-1}$. Table S3 shows the bulk and surface composition of the $\text{Au}/\text{Li}_3\text{PO}_4$ -13 samples with different loadings of Au. It should be noted that the Au cluster tends to be located on the outer surface of the Li_3PO_4 support. XRD patterns of $\text{Au}/\text{Li}_3\text{PO}_4$ -13 and Li_3PO_4 -x, as shown in Fig. S2, confirming that the structure of Li_3PO_4 is β form with orthorhombic symmetry [16,17], which does not change after gold deposition or pH adjustment. Additionally, metallic gold is not detected over $\text{Au}/\text{Li}_3\text{PO}_4$ -13 and $\text{Au}/\text{Li}_3\text{PO}_4$ 5 h, owing to the fact that

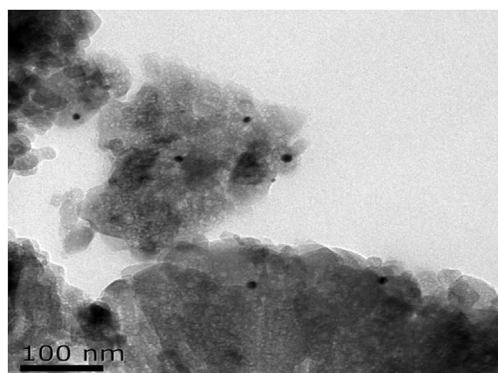


Fig. 1. TEM image of gold particles in fresh Au/Li₃PO₄-13.

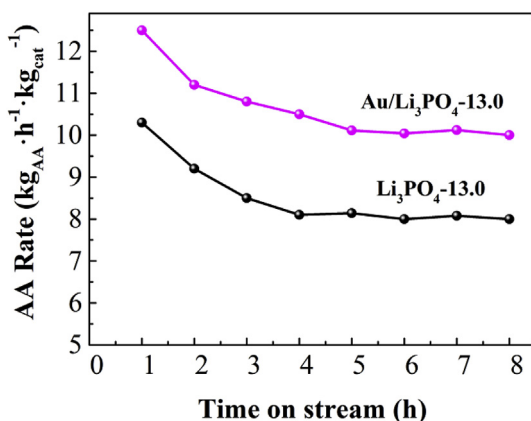


Fig. 2. Production yield of AA for Li₃PO₄-13 and Au/Li₃PO₄-13.

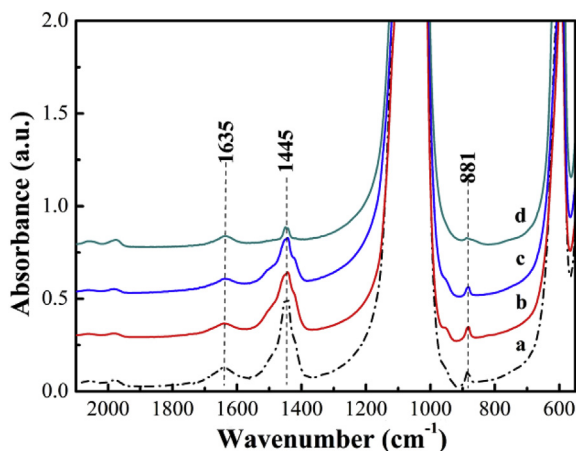


Fig. 3. The FT-IR spectra of (a) Au/Li₃PO₄-13, (b) Li₃PO₄-13, (c) Li₃PO₄-11 and (d) Li₃PO₄-9.

the gold content of Au/Li₃PO₄ is low (0.042 wt%) or the gold particles are well-dispersed on Li₃PO₄ [18].

Fig. S3 shows the UV-visible spectra of Au/Li₃PO₄-13 and Li₃PO₄-x. The absorption of visible light at 500–600 nm is due to the surface plasmon resonance band of gold nanoparticles [19,20]. Fig. S4 shows the ultraviolet-visible spectra of the rest of gold catalyst. The surface plasmon resonance band of gold nanoparticles (530 nm band) can be seen. Fig. 1 and Fig. S5 show the TEM images of Au/Li₃PO₄ samples with Au loadings of 0.042 wt% and 0.055 wt%, respectively. Black dots represent

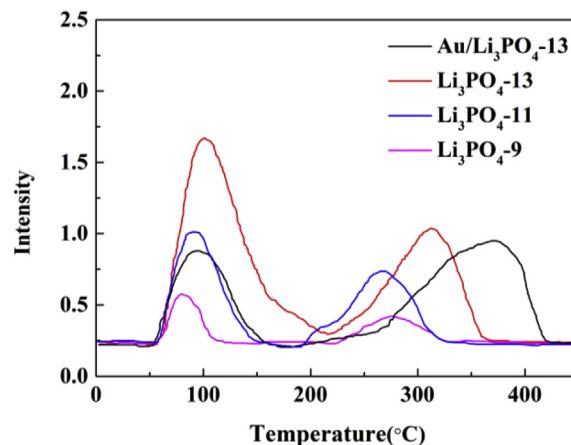


Fig. 4. The CO₂-TPD curves of Au/Li₃PO₄-13 and Li₃PO₄-x.

gold nanoparticles in the TEM image. Due to the low gold loading, only a small amount of metal particles can be seen [21]. It can be seen that the Au particles of Au/Li₃PO₄-0.042 with an average diameter of 11 nm are dispersed on the carrier. The Au particles of Au/Li₃PO₄-0.055 have an average diameter of 18 nm. However, the performance of Au/Li₃PO₄-0.055 is not the best, so it can be concluded that excess Au loading will form larger Au particles, which is detrimental to charge transfer and ultimately leads to a decrease in catalytic performance.

The catalytic performance of PO rearrangement on Li₃PO₄ and Au/Li₃PO₄ are shown in Fig. 2. Wang et al. reported that the AA rate of the Li₃PO₄ catalyst was 7.6 kg_{AA}·h⁻¹·kg_{cat}⁻¹ at 1 h. The AA rate of the Au/Li₃PO₄-13 catalyst was 12.5 kg_{AA}·h⁻¹·kg_{cat}⁻¹ at 1 h, improved by 39%. In addition, it can be seen that the performance of catalysts becomes stable after 5 h, and the AA rate of Au/Li₃PO₄-13 increases by 20% compared with Li₃PO₄-13.

3.2. Discussion of the active sites

3.2.1. Result of FT-IR

The surface group information of the catalysts can be easily acquired by FT-IR technique, as shown in Fig. 3. The peaks at 1100 and 600 cm⁻¹ are ascribed to the P–O antisymmetric stretching vibration and symmetric stretching vibration, respectively. The absorption peak at 1635 cm⁻¹ is ascribed to the scissor vibration of O–H (δ_{OH}), owing to the adsorption of water in the air. The peaks at 1445 and 881 cm⁻¹ are ascribed to the C–O stretching vibration and plane deformation vibration, respectively. This result demonstrates the existence of CO₃²⁻, which is due to the reaction of basic catalyst surface with CO₂ in the atmosphere. Because the sampling process was strictly controlled, the adsorption amount of CO₂ could be quantitatively compared. In order to quantitatively compare the amount of base site, the area of peaks at 1445 and 881 cm⁻¹ were integrated, respectively. The area of peak at 1445 cm⁻¹ is 24.8 for Au/Li₃PO₄-13, and those of Li₃PO₄-x (x = 13, 11 and 9) are 22.2, 14.4 and 1.6, respectively. The area of peak at 881 cm⁻¹ are 1.2, 1.1, 0.8 and 0.2 for Au/Li₃PO₄-13 and Li₃PO₄-x (x = 13, 11 and 9). As the pH decreases to 9, the two peaks attributed to CO₃²⁻ almost vanish, suggesting that the basicity of the surface is weakened. Unexpectedly, after the deposition of gold, the FT-IR absorption of CO₃²⁻ is not weakened. On the contrary, it is reinforced. It can be deduced that the deposition of gold may increase the base amount or the strength. In order to verify this, CO₂-TPD was employed to discuss the further information of activity enhancement.

Fig. S6 shows the FT-IR spectra of Au/Li₃PO₄-x with different Au Loading. As the Au loading increases, the peak area at 1445 and 881 cm⁻¹ gradually increases. It can be inferred that the Au loading has a positive effect on the increase of the basic site.

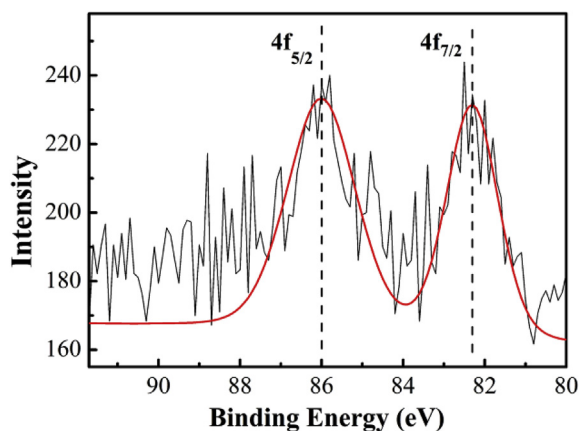


Fig. 5. XPS profiles of Au 4f region of Au/Li₃PO₄-13.

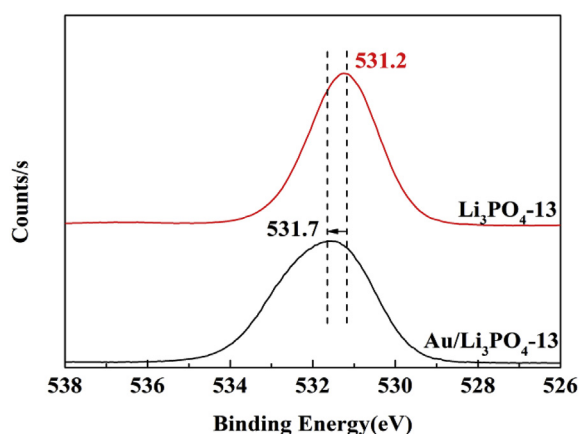


Fig. 6. XPS profiles of O 1s region of Au/Li₃PO₄-13.

3.2.2. Result of CO₂-TPD and NH₃-TPD

The profiles of Au/Li₃PO₄-13 and Li₃PO₄-x are shown in Fig. 4. There are two CO₂ desorption peaks in the profiles. For the Li₃PO₄-13, the first peak with T_{max} = 139 °C represents the weak base site and the second peak with T_{max} = 326 °C corresponds to the strong base site. However, for Au/Li₃PO₄-13, the peaks of weak and strong base sites are at 134 °C and 382 °C, respectively. In other words, weak base strength is not changed, but strong base strength is enhanced after gold deposition. Considering the pK values of H₃PO₄ (2.1,7.2,12.3), the prevalent ions in the solution changes with the decrease of pH values. For Li₃PO₄-11 and Li₃PO₄-9, as the monohydrogen and dihydrogen phosphate ions increase, both weak and strong base strength are weakened. In order to quantitatively compare the amount of base site, the peak area of Au/Li₃PO₄-13 and Li₃PO₄-x were integrated, respectively, as shown in Table S4. For Au/Li₃PO₄-13, the amount of weak base sites decreases, but the amount of strong base sites increases. Because strong base sites are favorable to improve the activity of basic catalysts [22], it can be concluded that the enhancement of catalytic activity comes from the improvement of the strength and amount of basic sites after gold deposition. As for the reason of this enhancement, we consider that gold species act as stronger base site and make it improve. XPS was employed to get further information.

Fig. S7 shows the CO₂-TPD curves of two Au/Li₃PO₄ catalysts with different calcination temperatures. It can be seen that the strong basic site of Au/Li₃PO₄ with higher calcination temperature is stronger, and the strong basic site is advantageous for catalyzing the rearrangement of propylene oxide, so the performance of Au/Li₃PO₄-300 is better.

Fig. S8 shows the NH₃-TPD curves for Li₃PO₄ catalysts of different pH values. It can be seen that there is no great difference in the amount of

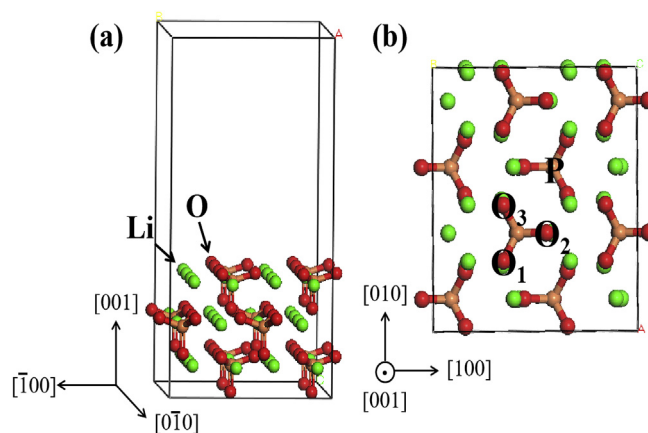


Fig. 7. (a) Surface structure of the Li₃PO₄ (001) surface, (b) Top view. The red balls represent oxygen atoms, green balls represent lithium atoms, orange balls represent phosphorus atoms. (For interpretation of the references to colour in this figure legend, the reader is referred to the Web version of this article.)

strong acid sites, and the amount of weakly acidic sites increases slightly with the decrease of pH, so the main reason for the change in performance is the change of the basic sites.

3.2.3. Result of XPS

XPS measurement is used to analyze the chemical state of elements so as to discuss the shifts of electron binding energy over Au/Li₃PO₄. Fig. 5 shows the XPS spectra of the Au 4f regions for Au/Li₃PO₄-13. There are two broad peaks at 86.0 and 82.3 eV (corresponding to the 4f_{7/2} and 4f_{5/2} peaks) for the Au element, which is consistent with the Au⁰ oxidation state [23]. The difference between these two peaks for gold (3.7 eV) is exactly the same as that of bulk Au⁰ [24–26]. However, the peak positions are slightly different from that of bulk Au⁰. The Au 4f_{5/2} peak of Au/Li₃PO₄ is seen to shift to lower binding energies by 1.7 eV than that of bulk Au⁰, which is reported to be at 84.0 eV [27,28]. This indicates that Au species is negatively charged after gold was deposited on Li₃PO₄.

Fig. 6 shows the XPS spectra of the O1s regions of Au/Li₃PO₄-13 and Li₃PO₄-13. It can be seen that the binding energy of the O1s spectra of Au/Li₃PO₄-13 relative to the O of Li₃PO₄-13 was increased by 0.5 eV. This indicates that the O species loses electrons after gold is deposited on Li₃PO₄. The cause of electron density changes of the O and Au should be further discussed.

Fig. S9 shows the XPS spectrum of the Li 1s (a) and P 2p (b) regions of Au/Li₃PO₄-x and Li₃PO₄-x. It can be seen that there is no change in the binding energy of Li and P of these catalysts. Fig. S10 is the XPS data for different Au loaded samples. It can be seen that the binding energy of Au of the samples with different Au loadings is reduced. However, it is worth noting that the binding energy of the sample with the highest Au loading is reduced by 1.5 eV, which is lower than the reduced binding energy of the sample with an Au loading of 0.042 wt%.

The Au 4f binding energy for supported catalysts compared with that in bulk Au has been investigated in a number of literatures [29–31]. Yejun Park et al. [32] proposed that in the Au/AlPO₄ nanocomposite, the shift of the Au 4f peaks occurs toward lower binding energies, indicating the presence of a negative charge on gold nanoparticles due to the electron transfer from AlPO₄. Caixia Qi et al. [33] have reported that the majority of the gold tends to be zero valence metal, but there is a small shift toward lower binding energy for three P-containing samples, implying the transfer of electrons to Au and the formation of Au^{δ-} atoms. However, the decrease in the Au 4f binding energy for Au/Li₃PO₄ has not been studied yet. In Fig. 5, Au 4f shifts to lower binding energy. In Fig. 6, O 1s shifts to a higher binding energy. It can be inferred that the decrease of the Au 4f binding energy may come from the charge transfer from the surface of Li₃PO₄. The interaction between gold and Li₃PO₄ results in a local perturbation of the electronic structure and a shift in the density of

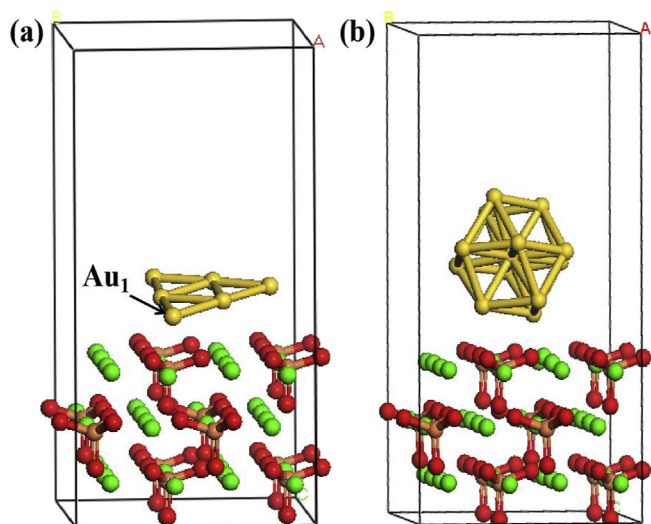


Fig. 8. Configuration of Au₆ (a) and Au₁₃ (b) cluster adsorption on the Li₃PO₄ (001) surface.

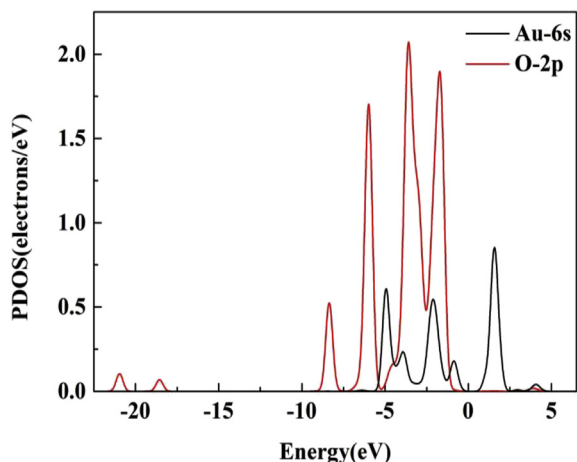


Fig. 9. PDOS of Au-6s and O-2p after Au₆ adsorption.

states as compared with bulk Au [34]. Because of electron-rich oxygen atoms and their high content, we considered that the charge transfers, most likely, from oxygen atoms to the gold cluster. The electron-rich Au acts as strong base sites, which promotes the catalytic activity.

3.2.4. Result of DFT

In order to verify the conclusion, we have performed structural relaxations at the level of DFT using the CASTEP simulation package. The calculations were done in the framework of the generalized gradient approximation, using projector-augmented wave pseudopotentials and the Perdew-Burke-Ernzerhof exchange-correlation energy [35]. We have used $3 \times 2\text{Li}_3\text{PO}_4$ (001) surface slab with a 15 Å vacuum spacing. The thickness of the slabs in the computational supercells is 7 layers, and the bottom two atomic layers were kept fixed during the structural relaxations to simulate the underlying bulk. Fig. 7 shows the optimized structure of the surface of Li₃PO₄. To describe the state of O and the distance from Au to the surface of Li₃PO₄, we selected a gold atom labeled Au₁ and labeled O as O₁, O₂ and O₃ on the surface of Li₃PO₄. In order to simplify the calculation and ensure that the interactions between the periodic images of the substrate-support, we chose a two-dimensional Au₆ cluster and a minimum cubic octahedron Au₁₃ cluster composed of 13 atoms as a model. The model is shown in Fig. 8. In all calculations, we used a plane-wave cutoff energy of 450 eV and sampled the Brillouin

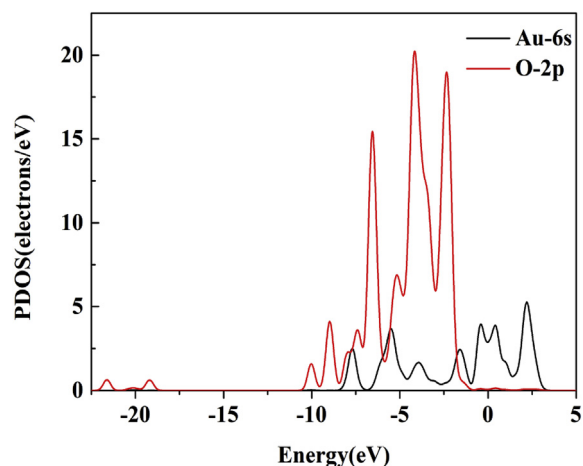


Fig. 10. PDOS of Au-6s and O-2p after Au₁₃ adsorption.

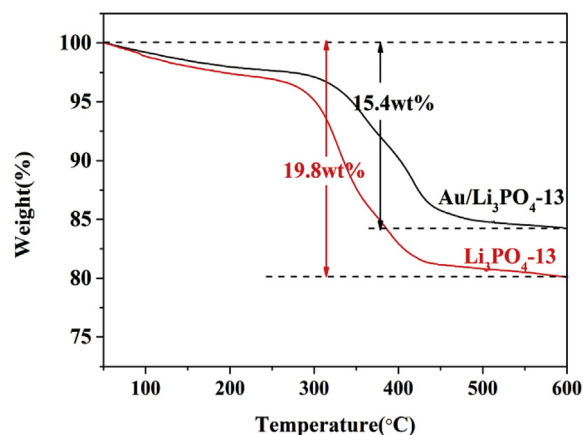


Fig. 11. TG curves of Li₃PO₄ and Au/Li₃PO₄-13.

zone only at the Γ point. The structural relaxations were terminated when the total energy of the slab converged to 0.001 eV. To better understand the trend in the atomic charge transfer between the gold and substrate, the net charge-transfer was calculated using Mulliken population analysis. The result is shown in Tables S5 and S6. We found that after gold adsorption on Li₃PO₄ (001), the Au₆ cluster gains 1.08 e. The charge of the O atom increases from -1.22 to -0.92 e. The Au₁₃ cluster gains 0.45 e. The charge of the O atom increases from -1.22 to -1.06 e. The PDOS (partial density of states) of Au-6s and O-2p after Au₆ and Au₁₃ adsorption are shown in Fig. 9 and Fig. 10. After the two clusters adsorbed on Li₃PO₄, the two orbitals have good overlap, which indicates that the electron transfer trend of the Au₁₃ clusters is consistent with that of Au₆.

In Table S7, we summarize the P-O bond and O-P-O bond angle of the surface O of the Li₃PO₄ unit cell before and after adsorption. Table S8 shows the distance of Au-Au before and after adsorption and the distance from our chosen Au atom to the surface of Li₃PO₄ unit cell. It can be seen from the table that the average bond length of the Au clusters before and after adsorption increases. The reason is that electrons are transferred from O atoms to gold. This electron transfer results in an increase in the average bond length of the Au cluster [36].

3.2.5. Result of TG and regeneration of deactivated catalyst

Fig. 11 shows the TG curves of Li₃PO₄ and Au/Li₃PO₄. The decomposition temperatures of the carbonaceous deposits of the two catalysts are basically the same, indicating that their carbonaceous sediments are similar in nature. The amount of carbonaceous deposits of Au/Li₃PO₄ is lower than that of Li₃PO₄. For many catalysts, carbonaceous deposits can

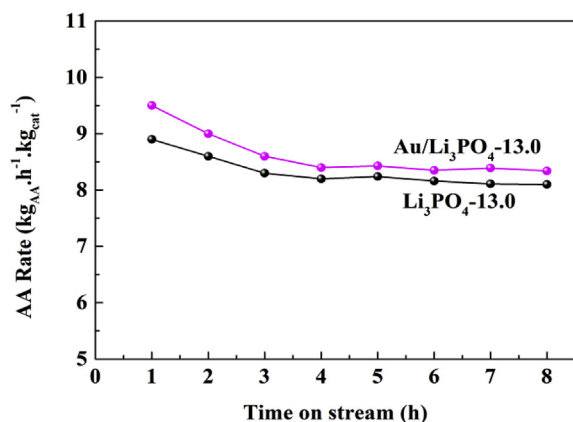


Fig. 12. Production yield of AA for Li₃PO₄-13 and Au/Li₃PO₄-13 after regeneration.

be removed, at least in part, by calcination in air. We use TG to determine the conditions under which carbonaceous deposits may be removed. It can be seen from Fig. 11 that most of the carbonaceous deposits react with air at a temperature of 300–400 °C, and the carbonaceous deposits are substantially decomposed at 400 °C. However, according to the previous studies, high calcination temperature would be bad for the performance of the Au-loaded catalyst, so we calcined the catalyst in air at 350 °C for 2 h to remove most of the carbonaceous deposits. The performance after regeneration is shown in Fig. 12. Compared to the fresh catalyst, the performance of Li₃PO₄ is reduced by 14%, while that of Au/Li₃PO₄ is reduced by 26%. This may be due to an increase in the particle size of the Au particles due to an increase in temperature, which affects the catalytic performance [37].

4. Conclusions

Au/Li₃PO₄ were synthesized via a deposition precipitation method. Li₃PO₄ with pH = 13 showed a higher catalytic performance. Compared to Li₃PO₄, the support of gold could improve the catalytic activity. Furthermore, Au/Li₃PO₄-13 with gold loading of 0.042 wt% which was calcined at 300 °C showed the best performance. This enhanced activity over Au/Li₃PO₄-13 has been discussed by FT-IR, CO₂-TPD, XPS and DFT. From the results of FT-IR and CO₂-TPD, it can be concluded that the enhancement might come from the strength and amount of strong basic sites after gold deposition. Results of XPS spectra and DFT further confirmed that the charge transferred from oxygen species to gold species, leading to the electron-rich gold species, which could act as stronger base sites.

Acknowledgements

The work is financed by the National Natural Science Foundation of

China (No.21276127) and the Priority Academic Program Development of Jiangsu Higher Education Institutions (PAPD).

Appendix A. Supplementary data

Supplementary data to this article can be found online at <https://doi.org/10.1016/j.jssc.2019.120922>.

References

- [1] A. Jamalian, B. Rathman, G.L. Borosky, K.K. Laali, *Appl. Catal. Gen.* 486 (2014) 1–11.
- [2] G. Neri, G. Rizzo, C. Crisafulli, L. De Luca, A. Donato, M.G. Musolino, R. Pietropaolo, *Appl. Catal. Gen.* 295 (2005) 116–125.
- [3] T. Imanaka, Y. Okamoto, S. Teranishi, *Bull. Chem. Soc. Jpn.* 45 (1972) 1353–1356.
- [4] C. Raptis, H. Garcia, M. Stratakis, *Angew. Chem. Int. Ed.* 48 (2009) 3133–3136.
- [5] M. Liang, et al., *Catal. Lett.* 149 (2019) 942–949.
- [6] E. Ruiz-Hitzky, B. Casal, *J. Catal.* 92 (1985) 291–295.
- [7] D.P. Serrano, R. van Grieken, J.A. Melero, A. Garcia, *Appl. Catal. Gen.* 269 (2004) 137–146.
- [8] L. Jiang, H. Li, Y. Wang, W. Ma, Q. Zhong, *Catal. Commun.* 64 (2015) 22–26.
- [9] M. Haruta, M. Date, *Appl. Catal. Gen.* 222 (2001) 427–437.
- [10] M. Haruta, N. Yamada, T. Kobayashi, S. Iijima, *J. Catal.* 115 (1989) 301–309.
- [11] M. Haruta, *Nature* 437 (2005) 1098–1099.
- [12] H.F. Yin, Z. Ma, H.G. Zhu, M.F. Chi, S. Dai, *Appl. Catal. Gen.* 386 (2010) 147–156.
- [13] A.S.K. Hashmi, G.J. Hutchings, *Angew. Chem. Int. Ed.* 45 (2006) 7896–7936.
- [14] M. Li, Z. Wu, Z. Ma, V. Schwartz, D.R. Mullins, S. Dai, S.H. Overbury, *J. Catal.* 266 (2009) 98–105.
- [15] Z. Li, Y. Wang, J. Zhang, D. Wang, W. Ma, *Catal. Commun.* 90 (2017) 87–90.
- [16] R.M. Rojas, J.L.M. De Vidales, A. Delgado, J.V. Sinisterra, *J. Solid State Chem.* 106 (1993) 237–252.
- [17] Y.A. Du, N. Holzwarth, *Phys. Rev. B* 76 (2007), 174302.
- [18] M. Hosseini, T. Barakat, R. Cousin, A. Aboukaïs, B.L. Su, G. De Weireld, S. Siffert, *Appl. Catal. B Environ.* 111 (2012) 218–224.
- [19] R. Zanella, S. Giorgio, C.-H. Shin, C.R. Henry, C. Louis, *J. Catal.* 222 (2004) 357–367.
- [20] S. Oros-Ruiz, R. Gómez, R. López, A. Hernández-Gordillo, J.A. Pedraza-Avella, E. Moctezuma, E. Pérez, *Catal. Commun.* 21 (2012) 72–76.
- [21] D. Horváth, L. Toth, L. Guzzi, *Catal. Lett.* 67 (2000) 117–128.
- [22] Y. Okamoto, T. Imanaka, S. Teranishi, *Bull. Chem. Soc. Jpn.* 46 (1973) 4–8.
- [23] M.P. Casaleto, A. Longo, A. Martorana, A. Prestianni, A.M. Venezia, *Surf. Interface Anal.* 38 (2006) 215–218.
- [24] A. Zwijnenburg, A. Goossens, W.G. Sloof, M.W.J. Crajé, A.M.V.D. Kraan, L.J.D. Jongh, M. Makkee, J.A. Moulijn, *J. Phys. Chem. B* 106 (2002) 9853–9862.
- [25] A.M. Venezia, L.F. Liotta, G. Pantaleo, V.L. Parola, G. Deganello, A. Beck, Z. Koppány, K. Frey, D. Horváth, L. Guzzi, *Appl. Catal. Gen.* 251 (2003) 359–368.
- [26] S.W. Han, Y. Kim, K. Kim, *J. Colloid. Interf. Sci.* 208 (1998) 272.
- [27] K. Takahiro, S. Oizumi, A. Terai, K. Kawatsura, *J. Appl. Phys.* 100 (2006) 314–325.
- [28] J.F. Moulder, W.F. Stickle, P.E. Sobol, K.D. Bomben, J. Chastain, R.C. King, *Physical Electronics USA Inc Minnesota*, 1992, p. 220.
- [29] P. Konova, A. Naydenov, C. Venkov, D. Mehandjiev, D. Andreeva, T. Tabakova, *J. Mol. Catal.* 213 (2004) 235–240.
- [30] P. Lignier, M. Comotti, F. Schüth, J.-L. Roussel, V. Caps, *Catal. Today* 141 (2009) 355–360.
- [31] J. Moma, M. Scurrell, W. Jordaán, *Top. Catal.* 44 (2007) 167–172.
- [32] Y. Park, B. Lee, C. Kim, J. Kim, S. Nam, Y. Oh, B. Park, *J. Phys. Chem. C* 114 (2010) 3688–3692.
- [33] C. Qi, H. Su, R. Guan, X. Xu, *J. Phys. Chem. C* 116 (2012) 17492–17500.
- [34] N. Kruse, S. Chenakin, *Appl. Catal. Gen.* 391 (2011) 367–376.
- [35] J.P. Perdew, K. Burke, M. Ernzerhof, *Phys. Rev. Lett.* 77 (1996) 3865–3868.
- [36] A. Abbasi, et al., *Surf. Sci.* 663 (2017) 35–46.
- [37] A. Tomoki, et al., *Surf. Interface Anal.* 31 (2001) 73–78.